A 900-MHz/1.8-GHz CMOS Transmitter for Dual-Band Applications

Behzad Razavi, *Member, IEEE*

***Abstract*— The design of a radio-frequency transmitter that can operate in two bands while employing a minimal number of external components entails many challenges at both the architecture and the circuit levels. This paper describes the design of a 900-MHz/1.8-GHz transmitter implemented in CMOS technology for dual-band applications. Configured as a two-step architecture, the circuit generates the first upconverted signal in quadrature form and subsequently performs single-sideband modulation to produce the output in two bands. Fabricated in a 0.6-μm digital CMOS technology, the transmitter exhibits unwanted spurs 40 dB below the carrier while drawing 75 mW from a 3-V supply.**

***Index Terms*—Gaussian minimum shift keying (GMSK) modulators, radio-frequency (RF) CMOS circuits, single-sideband (SSB) mixers, wireless transceivers.**

I. Introduction

THE availability of new frequency bands in the 1.8-GHz range and the proliferation of various wireless standards have motivated vigorous efforts in the area of multistandard transceivers. Providing both higher flexibility and roaming capability and increasing the overall capacity in mobile communications, dual-band operation has rapidly penetrated various radio-frequency products. However, cost and form factor considerations severely constrain the choice of the architecture and frequency planning as well as the design of the building blocks of such transceivers. In particular, the number of oscillators, frequency synthesizers, and external filters and resonators must be minimized.

This paper describes the design of a 900-MHz/1.8-GHz CMOS transmitter for dual-band applications, with emphasis on compatibility with the Global System for Mobile Communication (GSM) and Digital Communication System at 1800 MHz (DCS1800). Employing two upconversion steps, the circuit generates 900-MHz and 1.8-GHz outputs that can assume linear or nonlinear modulation depending on the type of signals applied to the baseband ports. A prototype fabricated in a digital 0.6-μm CMOS technology displays unwanted spurs 40 dB below the carrier while consuming 75 mW from a 3-V supply. To our knowledge, this is the first published work on a dual-band transmitter.

Section II of the paper deals with general issues in dual-band transmitters. Section III presents the transmitter architecture, and Section IV describes the design of the building blocks. Section V summarizes the experimental results.

Manuscript received September 7, 1998; revised December 18, 1998.

The author is with the Department of Electrical Engineering, University of California, Los Angeles, CA 90095 USA (e-mail: razavi@ee.ucla.edu).

Publisher Item Identifier S 0018-9200(99)03673-2.

TABLE I
System Characteristics of GSM and DCS1800

	GSM	DCS1800
Modulation	Gaussian Minimum Shift Keying	
Multiple Access	Time–Division Multiple Access	
Duplexing	Frequency–Division Duplexing	
Receive Band	935–960 MHz	1805–1880 MHz
Transmit Band	890–915 MHz	1710–1785 MHz
Channel Spacing	200 kHz	
Number of Channels	124	350

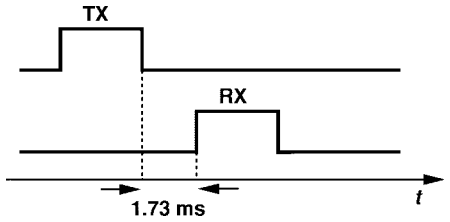

Fig. 1. Time offset between receive and transmit time slots.

II. General Considerations

In this design, the GSM and DCS1800 standards have been chosen as the framework. These standards incorporate the same modulation format, channel spacing, and antenna duplexing. Table I summarizes the characteristics of each standard, indicating that a dual-band transceiver can exploit the properties common to both so as to reduce the off-chip hardware.

To minimize the number of oscillators and synthesizers, the receivers and transmitters in a dual-band system must be designed concurrently, with the frequency planning chosen such that the receive and transmit paths are driven by the same synthesizers. Although GSM and DCS1800 use frequency-division duplexing (FDD) at the front end, their actual operation is somewhat similar to time-division duplexing (TDD) because their receive and transmit time slots are offset by 1.73 ms (three time slots) (Fig. 1). Thus, frequency synthesizers can be time-shared between the receiver and the transmitter.

The dual-band transmitter described herein is designed in conjunction with the dual-band receiver reported in [1]. To address the frequency planning issues, we briefly look at the receiver (Fig. 2). Based on the Weaver image-reject architecture [2], the receiver performs the first downconversion such that the GSM and DCS1800 bands appear as images of each other. The Weaver topology then selects one band and rejects the other by addition or subtraction of the spectra at points A and B. The first local oscillator (LO) frequency

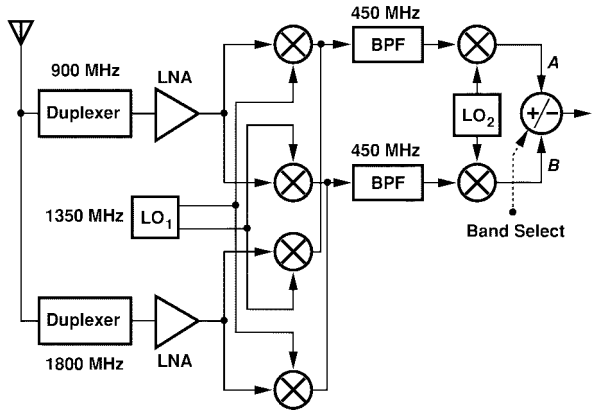

Fig. 2. Dual-band receiver architecture.

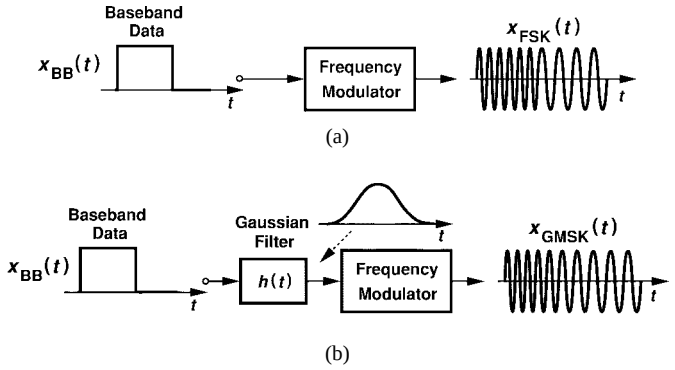

Fig. 3. Generation of FSK and GMSK signals.

is therefore equal to 1350 MHz—midway between the two bands—and the second LO frequency is in the vicinity of 450 MHz. To minimize the number of LO's and synthesizer loops, it is desirable to utilize the same frequencies for the transmit path as well.

Before considering suitable transmitter architectures, we review Gaussian minimum shift keying (GMSK) modulation to arrive at some of the design implications. Fig. 3 conceptually illustrates frequency shift keying (FSK) and GMSK. In FSK, rectangular baseband pulses are directly applied to a frequency modulator, e.g., a voltage-controlled oscillator (VCO), thereby creating an output waveform given by

$$x_{\mathrm{FSK}}(t) = A\cos\left[\omega_c t + K_0 \int x_{\mathrm{BB}}(t)\,dt\right] \qquad (1)$$

where K_0 is a constant denoting the "depth" of modulation and $x_{\mathrm{BB}}(t)$ represents the baseband signal.

An important drawback of FSK is the large bandwidth occupied by the modulated signal, partly because of the abrupt transitions in the frequency introduced by the sharp edges of the baseband pulses. We expect that if the frequency changes more smoothly from one bit to the next, then the required bandwidth decreases. In fact, the spectrum of the signal expressed by (1) decays in proportion to $f^{2(n+3)}$, where n denotes the highest continuous derivative of $x_{\mathrm{BB}}(t)$ [3]. Based on this observation, GMSK modulation alters the shape of the baseband pulses so as to vary the frequency gradually. As shown in Fig. 3(b), the rectangular pulses are first applied to a

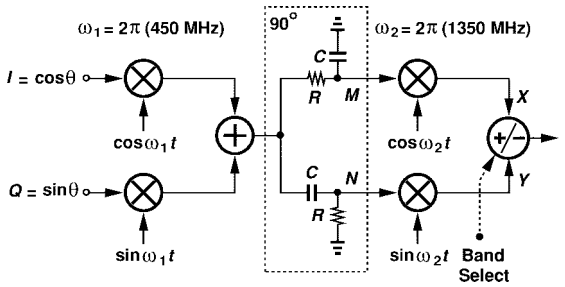

Fig. 4. Simple dual-band transmitter.

Gaussian filter, thereby generating smooth edges at the input of the frequency modulator. The resulting output is expressed as

$$x_{\mathrm{GMSK}}(t) = A\cos\left[\omega_c t + K_0 \int x_{\mathrm{BB}}(t) * h(t)\,dt\right] \qquad (2)$$

where $h(t) = \exp(-t^2/\tau^2)$ is the impulse response of the Gaussian filter.

The conceptual method described by Fig. 3(b) and (2) is indeed employed in some transmitters, e.g., for the Digital European Cordless Telephone standard. However, if the amplitude of the baseband signal applied to the VCO or the gain of the VCO are poorly controlled, so is the bandwidth of the modulated signal. For this reason, in high-precision systems such as GSM, the waveform in (2) is rewritten as

$$x_{\mathrm{GMSK}}(t) = A\cos\omega_c t\cos\theta - A\sin\omega_c t\sin\theta \qquad (3)$$

where $\theta = K_0 \int x_{\mathrm{BB}}(t) * h(t)\,dt$, and $\cos\theta$ and $\sin\theta$ are generated by accurate mixed-signal techniques [5], [6]. Equation (3) forms the basis for our transmitter design.

III. Transmitter Architecture

To employ 450- and 1350-MHz LO frequencies, we postulate that the transmitter must incorporate two upconversion steps: from baseband to an intermediate frequency (IF) of 450 MHz and from 450 to 900 MHz or 1.8 GHz. We also recognize that a simple mixer driven by the 450-MHz IF and the 1350-MHz LO generates the 900-MHz and 1.8-GHz signals with *equal* amplitudes, necessitating substantial filtering to suppress the unwanted component. It is therefore desirable to perform the second upconversion by single-sideband (SSB) mixing.

With the foregoing observations, we consider the topology shown in Fig. 4 as a possible solution. The baseband I and Q signals are upconverted to 450 MHz and subsequently separated into quadrature phases by means of an RC–CR network, resulting in $V_M = A\cos(\omega_1 t - \theta - \pi/4)$ and $V_N = A\sin(\omega_1 t - \theta - \pi/4)$. Single-sideband mixing of the IF and the second LO signals is then carried out by two mixers, with their outputs added or subtracted so as to produce the 900- or 1800-MHz output according to the band select command.

The architecture of Fig. 4 provides a compact solution for dual-band operation, but it suffers from several drawbacks. First, the RC–CR network introduces a loss of 3 dB in the signal path, and, more important, loads the first upconverter. Second, both of the outputs appear at the same port, making it difficult to utilize narrow-band tuned amplification at this

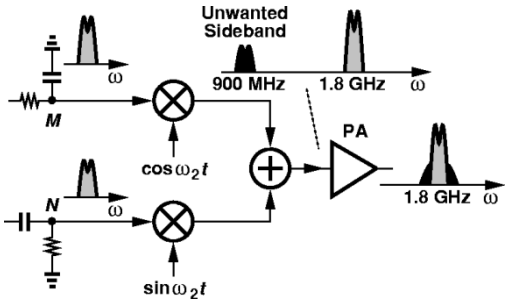

Fig. 5. Effect of unwanted sideband on DCS1800 output.

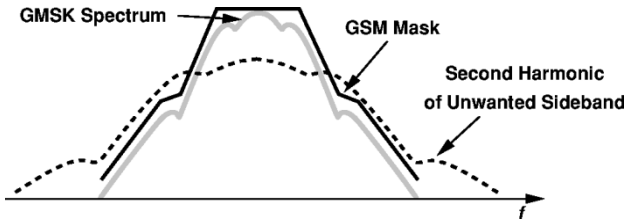

Fig. 6. Increase in adjacent-channel power due to second harmonic of unwanted sideband.

port. Third, even with perfect matching between the quadrature paths in the SSB mixer, the variation of the absolute value of RC with process and temperature leads to considerable amplitude mismatch between V_M and V_N, thereby creating a significant unwanted sideband at the output. For example, a 20% error in RC results in an unwanted sideband only 20 dB below the wanted component.

The existence of an unwanted sideband 900 MHz away from the desired signal may seem unimportant because various filtering operations in the following power amplifier (PA) and matching network provide further suppression. However, second-order distortion in the PA—a significant effect because PA's are typically single ended—may lead to a troublesome phenomenon in the generation of DCS1800 signals. Illustrated in Fig. 5, the issue arises because the second harmonic of the 900-MHz sideband falls in the transmitted DCS1800 channel. Since, from Carson's rule [4], the second harmonic of a frequency-modulated signal occupies roughly twice as much bandwidth as the first harmonic, the 1800-MHz output may exhibit substantial adjacent-channel power, violating the transmission mask (Fig. 6). Thus, the unwanted sideband produced by the SSB mixer must be sufficiently small.

In summary, the architecture of Fig. 4 requires two modifications: 1) the IF quadrature generation must avoid the use of RC–CR networks and 2) the GSM and DCS1800 paths must be separated at some point such that each can incorporate narrow-band tuning.

To produce the quadrature phases of the 450-MHz IF signal, we recognize that the *baseband* signal is available in quadrature phases, namely, $\cos\theta$ and $\sin\theta$ in (3). The IF signal can thus be generated in quadrature form as depicted in Fig. 7, where proper choice of the phases together with addition or subtraction at the output yields both $\cos(\omega_1 t+\theta)$ and $\sin(\omega_1 t+\theta)$. Compared to the circuit of Fig. 4, this configuration both provides higher gain balance between the two

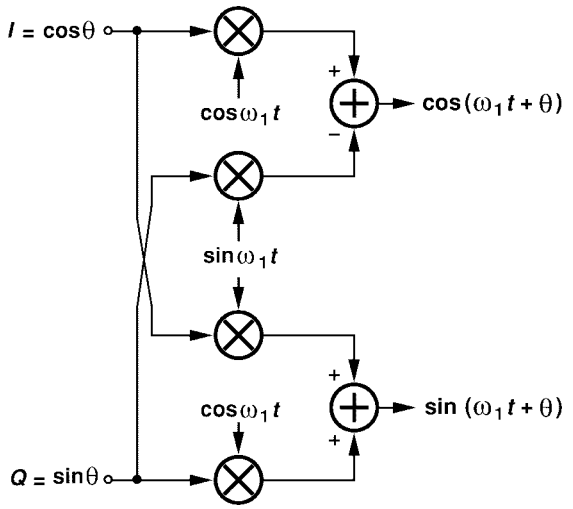

Fig. 7. Upconversion with quadrature outputs.

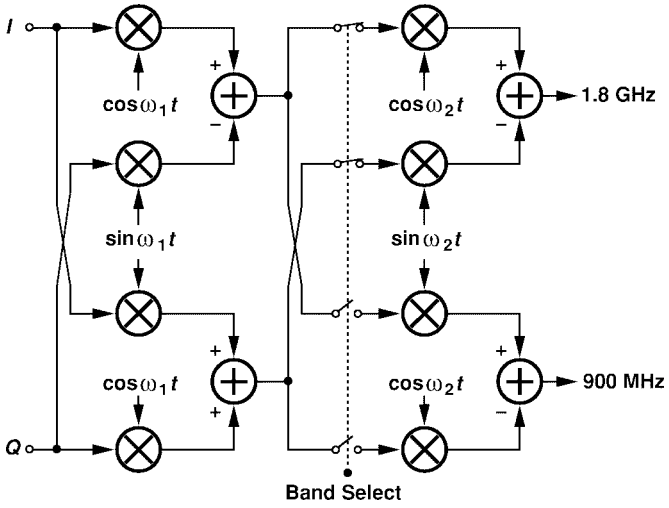

Fig. 8. Two-step upconversion generating 900-MHz and 1.8-GHz outputs.

paths and avoids the loss and loading of the RC–CR network while using two more mixers. The additional mixers consume more power, but since the conversion gain is higher in this case, the following SSB mixers require less power, leading to an overall power dissipation comparable to that of Fig. 4.

The 450-MHz outputs of the first upconverter can now be multiplied by the quadrature phases of the second LO and added or subtracted to generate the GSM and DCS1800 signals. As mentioned above, it is preferable to design the second upconversion modulators such that the 900-MHz and 1.8-GHz waveforms appear at the outputs of two different circuits, thus allowing efficient narrow-band amplification. This is accomplished as shown in Fig. 8, where two independent SSB modulators produce the two bands according to the band select command. Note that narrow-band tuning also suppresses the unwanted sideband resulting from mismatches in the SSB mixers. To save power consumption, only one of the modulators is active in either mode.

The overall architecture of the dual-band transmitter is shown in Fig. 9. Since all of the signals up to ports A and B are differential, each band incorporates a differential to

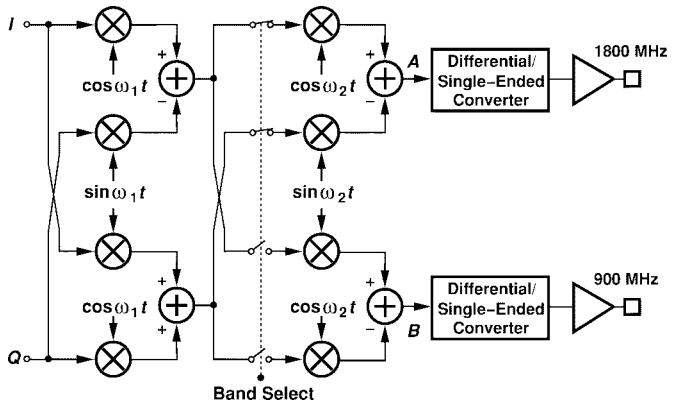

Fig. 9. Dual-band transmitter architecture.

single-ended (D/SE) converter, applying the result to an output buffer. The transmitter requires external power amplifiers to deliver the high power levels specified by GSM and DCS1800.

IV. Building Blocks

In this section, we describe the transistor-level implementation of each building block, emphasizing the design constraints imposed by the architecture. The circuit topologies are identical for both bands, but device dimensions and bias currents are chosen to optimize the performance of each.

A. First Upconversion

The 450-MHz upconversion modulator consists of two Gilbert cell mixers whose outputs are added in the current domain. Shown in Fig. 10, the circuit utilizes resistive source degeneration, thereby improving the linearity in the baseband port of each mixer. Two 100-nH inductors convert the output current to voltage. To minimize the area occupied by each inductor, a stack of three spiral structures made of three metal layers [Fig. 10(b)] is used [1], reducing the area by approximately a factor of eight [7]. Since the polysilicon connection and the bottom spiral suffer from substantial parasitic capacitance to the substrate, this node is connected to the supply voltage, increasing the self-resonance frequency of the inductor. The quality factor of the inductor is estimated to be about four, and the self-resonance frequency is about 600 MHz.

Why must the baseband ports be linearized? Let us return to (3) with the assumption that $\cos\theta$ and $\sin\theta$ experience third-order distortion. The resulting IF signal can then be expressed as

$$x_{\mathrm{GMSK}}(t) = A\cos\omega_c t[\cos\theta + \alpha\cos(3\theta)] - A\sin\omega_c t[\sin\theta + \alpha\sin(3\theta)] \quad (4)$$

where α represents the amount of third-order nonlinearity. Grouping the terms in (4), we obtain

$$x_{\mathrm{GMSK}}(t) = A\cos\left[\omega_c t + K_0\int x_{\mathrm{BB}}(t) * h(t)\,dt\right] + \alpha A\cos\left[\omega_c t + 3K_0\int x_{\mathrm{BB}}(t) * h(t)\,dt\right]. \quad (5)$$

Equation (5) reveals that third-order distortion gives rise to a component centered around ω_c but with a modulation index three times that of the ideal GMSK signal. Invoking Carson's rule, we postulate that the second term occupies roughly three times the bandwidth, raising the power transmitted in adjacent channels. Fig. 11 shows the simulated spectra of the two components in (5) with $\alpha = 1$, indicating that the

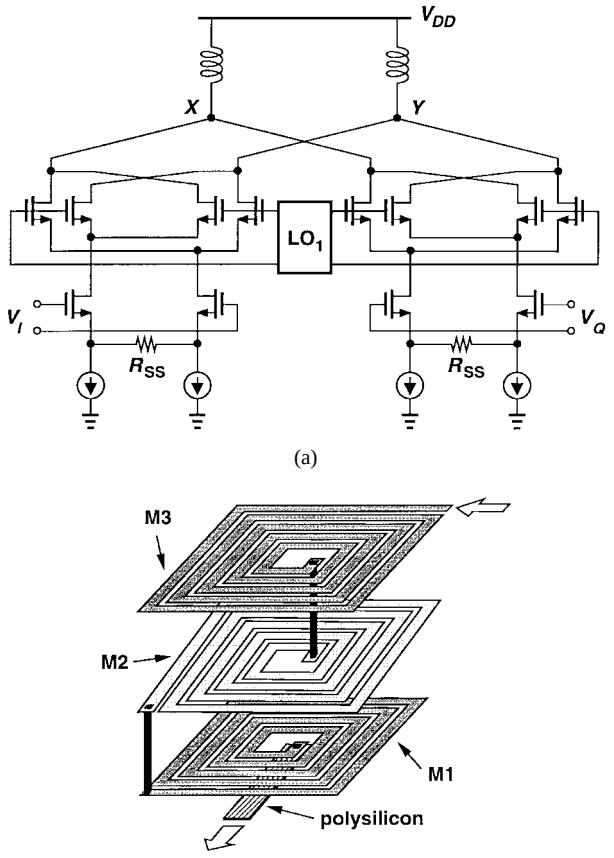

(a)

(b)

Fig. 10. (a) First upconversion modulator and (b) implementation of load inductors.

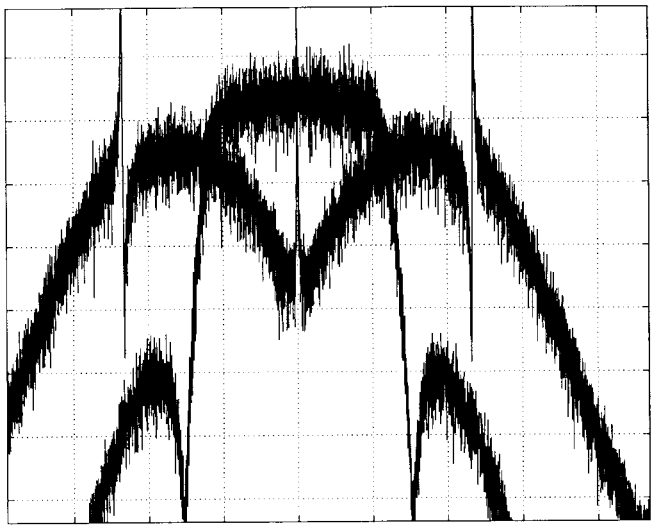

Fig. 11. Simulated spectra of the two terms in (5) (horizontal scale normalized to bit rate; vertical scale 5 dB/div.).

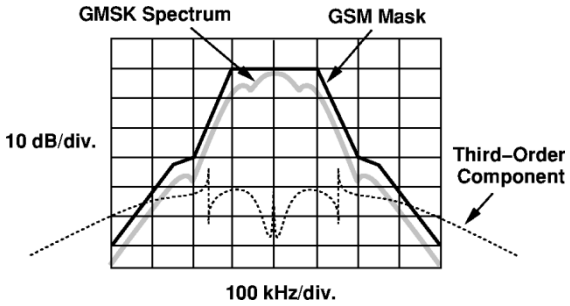

Fig. 12. Effect of harmonic distortion at baseband ports.

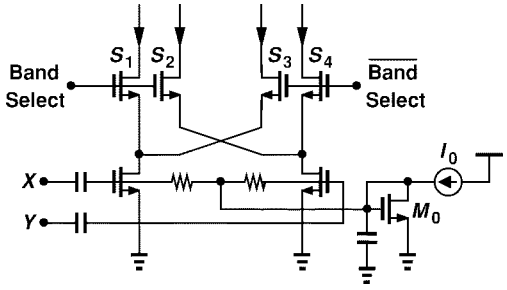

Fig. 13. Voltage-to-current converter with output switching.

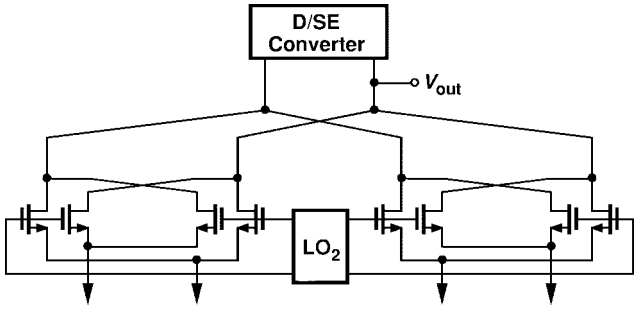

Fig. 14. Single-sideband modulator circuit.

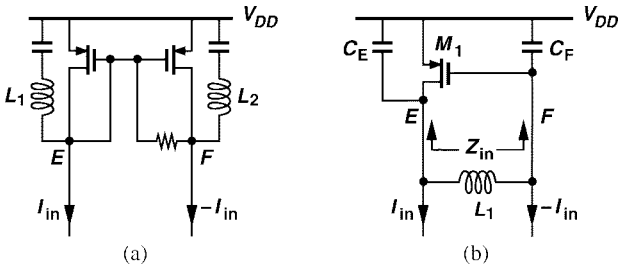

Fig. 15. Differential to single-ended conversion using (a) tuned current mirror and (b) negative resistance generator.

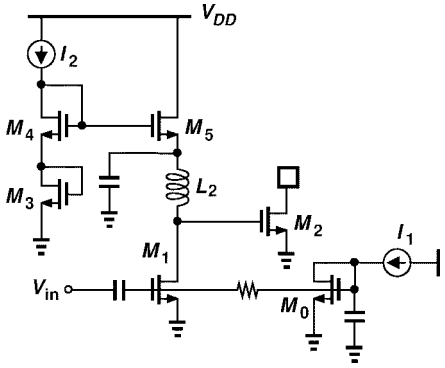

Fig. 16. Output buffer.

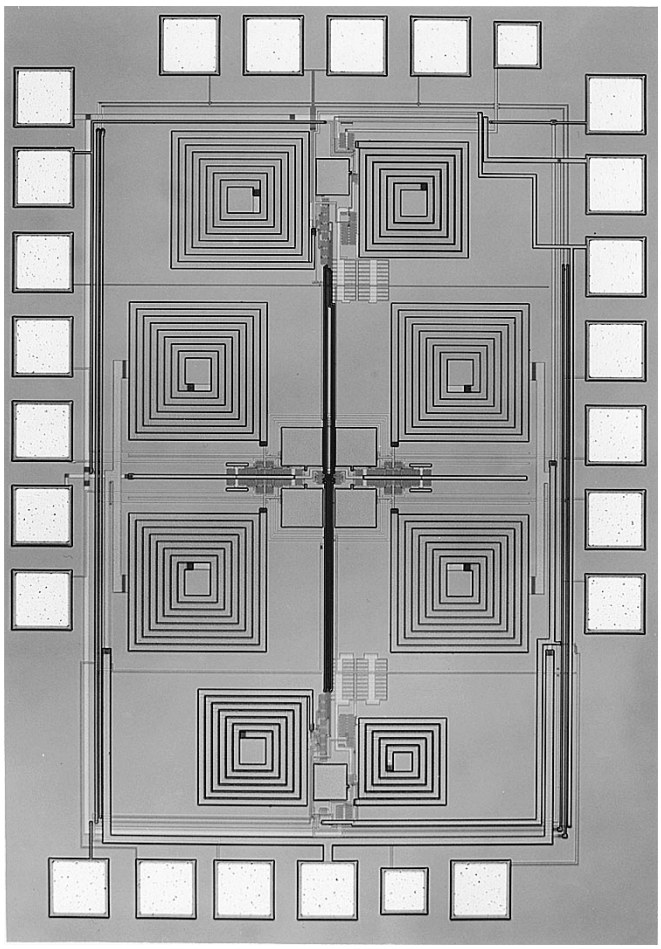

Fig. 17. Transmitter die photograph.

unwanted signal indeed consumes a wider band. For this reason, as depicted in Fig. 12, α must be small enough that the transmission mask is not violated. In this design, the resistive degeneration and tail currents are chosen so as to ensure $\alpha \approx 0.01$ with a 0.5-V_{PP} baseband input, yielding a third-order component 40 dB below the desired signal.

B. SSB Modulator

The signals generated at nodes X and Y in Fig. 10 must be "routed" to one of the SSB modulators according to the band select command. As illustrated in Fig. 13, the routing is performed in the current domain to minimize signal loss due to addition of the switches. Capacitively coupled to the output of the 450-MHz upconverter, the voltage-to-current converter employs grounded-source input devices to save the voltage headroom otherwise consumed by a tail current source. The bias current of the circuit is defined by M_0 and I_0. Note that S_1–S_4 operate in the deep triode region, sustaining a small voltage drop. Also, the linearity of this and subsequent stages is not critical because GMSK signals display a constant envelope and are quite insensitive to spectral regrowth [6].

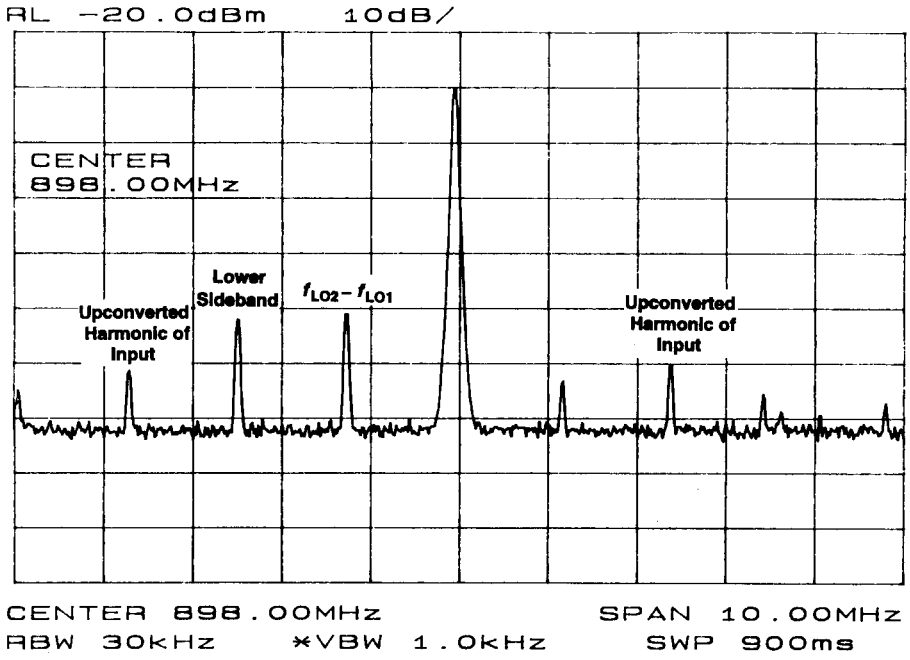

(a)

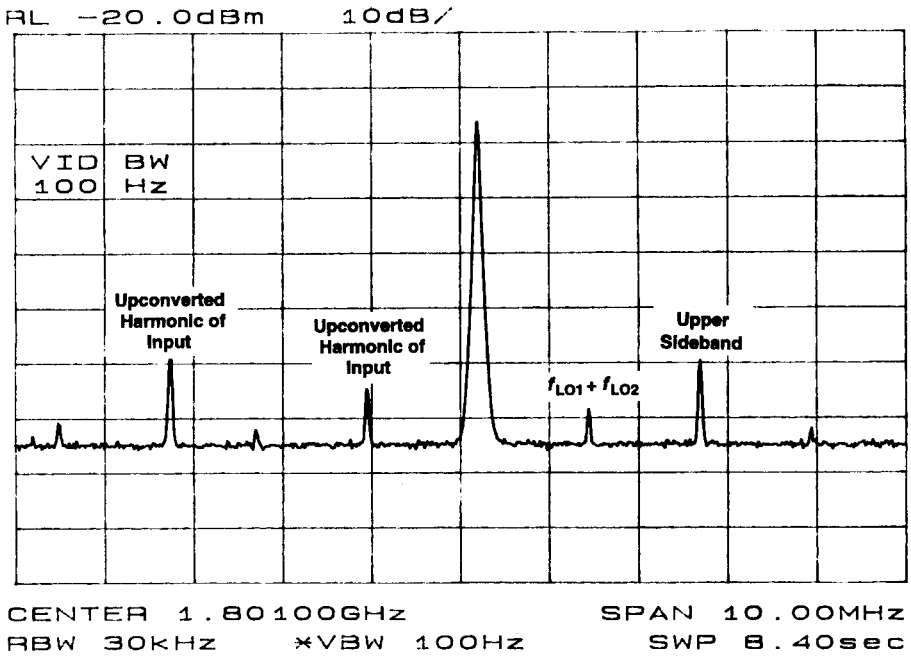

(b)

Fig. 18. Measured output spectrum at (a) 898 MHz and (b) 1.8 GHz (horizontal 1 MHz/div.; vertical 10 dB/div.).

With the quadrature phases of the IF signal available in the current domain, SSB mixing assumes a simple topology. Shown in Fig. 14, the circuit senses the differential current signals routed from each 450-MHz upconverter, performs mixing with the second LO, adds the resulting currents with proper polarity, and converts the output to single-ended form.

C. Differential to Single-Ended Converter

To achieve a reasonable gain, it is desirable to employ tuning in the D/SE converter. Fig. 15 depicts two realizations of such a circuit. In Fig. 15(a), a current mirror together with two inductors creates resonance at nodes E and F, reducing the effect of device capacitances. The difficulty here is the large gate-source capacitance of the two PMOS devices, mandating a small value for L_1 and hence a low conversion gain. Fig. 15(b) presents an alternative topology where a PMOS device introduces a negative resistance in parallel with a floating inductor. It can be shown that

$$Z_{\text{in}} = \frac{g_{m1}}{C_E C_F s^2} + \frac{1}{C_E s} + \frac{1}{C_F s} \tag{6}$$

where C_E and C_F denote the total capacitance at nodes E

and F, respectively [6]. As a compromise between margin to oscillation and boost in gain, the negative resistance, $-g_{m1}/(C_E C_F \omega^2)$, is chosen to increase the Q of the inductor by approximately a factor of two. Note that L_1 can assume a relatively large value because it sees C_E and C_F in *series*. In this design, the signal is sensed at F because this port exhibits a lower output impedance. Simulations indicate that the topology of Fig. 15(b) provides about three times the voltage gain of the circuit in Fig. 15(a).

D. Output Buffer

The output buffer is shown in Fig. 16. Two common-source stages, M_1 and M_2, boost the signal level, driving the 50-Ω impedance of the external instrumentation. The bias current of M_1 is defined by I_1 and M_0, and that of M_2 by I_2 and M_3. Neglecting the dc drop across the inductor, we have $V_{GS3} + V_{GS4} = V_{GS5} + V_{GS2}$; that is, I_{D2} can be ratioed with respect to I_2.

V. Experimental Results

The dual-band transmitter has been fabricated in a 0.6-μm CMOS technology. Fig. 17 shows a photograph of the die, which measures 1300 $\times$ 850 μm^2. All of the inductors are integrated with no additional processing steps.

The prototype is directly mounted on a printed circuit board and tested with a 3-V supply. The baseband signal consists of quadrature phases of a 1.2-MHz sinusoid, and the quadrature phases of LO_1 and LO_2 are generated by external couplers.

Fig. 18(a) shows the measured output spectrum when the 900-MHz band is selected. In addition to the desired component, the spectrum exhibits spurs corresponding to $f_{LO_2} - f_{LO_1}$, the lower sideband (resulting from mismatches in the first upconverter), and upconverted harmonics of the baseband signal. Similarly, as shown in Fig. 18(b), the 1.8-GHz output contains spurs at $f_{LO_1} + f_{LO_2}$, the upper sideband, and harmonics of the baseband input. Note that in both cases, the spurious components are at least 40 dB below the carrier. The circuit dissipates 75 mW, of which 10 mW is drained by the four upconversion mixers, 10 mW by the SSB mixer, and 55 mW by the output buffer.

Two aspects of these results should be revisited for GSM/DCS1800 applications. First, the output level is relatively low, necessitating an additional buffer prior to the power amplifier. Second, from the plots of Fig. 18(a) and (b), the thermal noise at large frequency offsets is approximately equal to -107 dBc/Hz at 900 MHz and -104 dBc/Hz at 1.8 GHz, requiring that the front-end duplexer filter provide adequate suppression of this noise in the receive band.

TABLE II
Performance of Dual-Band Transmitter

Output Frequency	900 MHz/1.8 GHz
Unwanted Sidebands	<–40 dBc
Power Dissipation	75 mW
Supply Voltage	3 V
Area	1.3 mm x 0.85 mm
Technology	0.6–μm CMOS

Table II summarizes the performance of the dual-band transmitter.

VI. Conclusion

The design of dual-band transmitters poses many challenges in terms of frequency planning and compatibility with their corresponding receivers. A two-step transmitter architecture has been introduced that provides dual-band operation with 450- and 1350-MHz LO frequencies. Also, circuit techniques for the generation of the quadrature phases of the IF signal as well as differential to single-ended conversion are presented.

Acknowledgment

The author wishes to thank R. Thiara for simulation results of Fig. 11.

References

[1] S. Wu and B. Razavi, "A 900-MHz/1.8-GHz CMOS receiver for dual-band applications," *IEEE J. Solid-State Circuits*, vol. 33, pp. 2178–2185, Dec. 1998.
[2] D. K. Weaver, "A third method of generation and detection of single-sideband signals," *Proc. IRE*, vol. 44, pp. 1703–1705, Dec. 1956.
[3] J. B. Anderson, T. Aulin, and C.-E. Sundberg, *Digital Phase Modulation.* New York: Plenum, 1986.
[4] L. W. Couch, *Digital and Analog Communication Systems*, 4th ed. New York: Macmillan, 1993.
[5] K. Feher, *Wireless Digital Communications.* Englewood Cliffs, NJ: Prentice-Hall, 1995.
[6] B. Razavi, *RF Microelectronics.* Upper Saddle River, NJ: Prentice-Hall, 1998.
[7] R. B. Merril *et al.*, "Optimization of high Q inductors for multi-level metal CMOS," in *Proc. IEDM*, Dec. 1995, pp. 38.7.1–38.7.4.

Behzad Razavi (S'87–M'90), for a photograph and biography, see p. 276 of the March 1999 issue of this Journal.